

Energy dependent ℓ -wave confinement-induced resonances

Benjamin Heß,^{1,*} Panagiotis Giannakeas,^{1,†} and Peter Schmelcher^{1,2,‡}

¹*Zentrum für Optische Quantentechnologien, Universität Hamburg,
Luruper Chaussee 149, 22761 Hamburg, Germany*

²*The Hamburg Centre for Ultrafast Imaging, Universität Hamburg,
Luruper Chaussee 149, 22761 Hamburg, Germany*

(Dated: December 3, 2024)

The universal aspects of two-body collisions in the presence of a harmonic confinement are investigated for both bosons and fermions. The main focus of this study are the confinement-induced resonances (CIR) which are attributed to different angular momentum states ℓ and we explicitly show that in alkaline collisions only four universal ℓ -wave CIRs emerge. Going beyond the single mode regime the energy dependence of ℓ -wave CIRs is studied. In particular we show that all the ℓ -wave CIRs may emerge even when the underlying two-body potential cannot support any bound state. We observe that the intricate dependence on the energy yields resonant features where the colliding system within the confining potential experiences an effective free-space scattering. Our analysis is done within the framework of the generalized K -matrix theory and the relevant analytical calculations are in very good agreement with the corresponding ab initio numerical scattering simulations.

PACS numbers: 34.10.+x, 03.75.-b, 34.50.-s

I. INTRODUCTION

In low-dimensional ultracold gases the manipulation of two-body collisions precludes the experimental realization of exotic many-body phases, such as the Tonks-Girardeau and the super-Tonks-Girardeau gas phases [1–3]. The concept of reduced dimensionality possesses a central role in these systems providing additional means to control the corresponding collisional events apart from the usual toolkit of Fano-Feshbach resonances [4–6]. More specifically, it was shown that free space non-resonant collisional events can be enhanced in the presence of waveguide-like trapping potentials [7, 8]. This yields a particular type of Fano-Feshbach resonance, the so-called confinement-induced resonances (CIRs) which occur when the scattering length is of the order of the length of the transversal confinement [9, 10]. Recent experimental advances allowed to explore the corresponding physics of CIRs in quasi-one- and quasi-two-dimensional (quasi-1D and quasi-2D) waveguide geometries [11–15] or in mixed dimensional scattering processes [16]. Complementing the experimental studies, substantial theoretical efforts exhibit a kaleidoscope of confinement-induced processes, such as dual [17] and higher partial wave CIRs [18, 19], multichannel [20–23] or anharmonic CIRs [24–26] and CIR molecule formation [27] or dipolar CIRs [28–30]. Further studies on CIR effects focus on the impact of various confining geometries, such as quasi-2D either harmonic [31, 32] or square well [33], and lattice potentials [34–36], or collisions in mixed dimensions [37]. Evidently, most of the theoretical efforts focus either on single par-

tial wave collisions or on the low energy regime. Therefore, extending the concept of mutually coupled higher partial wave CIRs to the regime of strong energy dependence and investigating their universal properties will elucidate the underlying collisional physics.

In this work, we consider two-body collisions of either bosonic or fermionic symmetry in the presence of an axially symmetric and harmonic waveguide. The atoms are allowed to perform collisions with higher partial waves where we take into account that the total colliding energy is well above the threshold of the ground state of the transversal confinement. The theoretical conceptualization of the corresponding resonant phenomena is based on a *fully* analytical and non-perturbative framework of the K -matrix approach [19, 28] including appropriate interatomic interactions with e.g. a van der Waals tail. This approach provides a generalization of the works of Granger *et al* [18] and Kim *et al* [38] incorporating however *all* the higher partial waves and contributions from *all* the closed channels. Furthermore, going beyond the previous studies we derive the connection of the *physical* K -matrix with all the relevant scattering observables obtaining thus the *full* scattering wave function. Therefore, the K -matrix approach can be applied equivalently to other systems, e.g. distinguishable or identical particles for various confining geometries or multichannel collisions beyond the single mode regime. Investigating the universal properties of the ℓ -wave CIRs for alkali atoms we observe that only four are present, namely s - (p -) and d - (f -) wave for bosons (fermions) due to the interplay between the confinement and the van der Waals potential. In addition, we study the energy dependence of the corresponding CIRs and observe that all the CIRs can occur even when the two-body potential cannot sustain a weakly bound or quasi-bound state. Moreover, for the energy dependent d - and f -wave CIRs we observe the

* bhess@physnet.uni-hamburg.de

† pgiannak@physnet.uni-hamburg.de

‡ pschmelc@physnet.uni-hamburg.de

bosonic and fermionic counterpart of the dual CIR [17], i.e. total transparency ($T = 1$), which occurs due to the destructive interference of $s - d$ and $p - f$ wave scattering, respectively. Finally, ab initio numerical simulations corroborate all the relevant analytical calculations within the K -matrix framework.

In detail, this paper is organized as follows. In Sec. II we introduce the waveguide Hamiltonian under consideration, define the interatomic potential and discuss the relevant theoretical methods, namely the K -matrix theory for quasi-1D waveguide geometries. The connection between the physical K -matrix and the physical observables is the content of Sec. III, while Sec. IV is devoted to the discussion of the universal properties of interatomic potential exhibiting a van der Waals tail and how this affects the CIRs in neutral diatomic collisions. A summary and conclusions are given in Sec. V.

II. WAVEGUIDE HAMILTONIAN AND K -MATRIX APPROACH

We consider the collision of two identical particles within a harmonic waveguide. Due to the harmonicity of the confinement we can separate the Hamiltonian into a part describing the center of mass and relative motion, respectively. The Hamiltonian of the relative motion relevant to the collisional process reads

$$H = \frac{-\hbar^2}{2\mu}\Delta + \frac{1}{2}\mu\omega_{\perp}^2\rho^2 + V_{LJ}(\mathbf{r}), \quad (1)$$

where $r = \sqrt{z^2 + \rho^2}$ is the interparticle distance, with z and ρ describing the longitudinal and transversal degrees of freedom, respectively. μ denotes the reduced mass of the colliding pair and ω_{\perp} is the confinement frequency. Accordingly, the harmonic oscillator length scale is given by $a_{\perp} = \sqrt{\hbar/\mu\omega_{\perp}}$. The term $V_{LJ}(r) = \frac{C_{10}}{r^{10}} - \frac{C_6}{r^6}$ is the Lennard-Jones 6-10 potential indicating the short-ranged two-body interatomic interactions. C_6 is the dispersion coefficient and it defines the van der Waals length scale via the relation $\beta_6 = (2\mu C_6/\hbar^2)^{1/4}$. We set C_{10} as a parameter in order to tune the corresponding scattering lengths induced by the short-range potential. Among others, the particular choice $V_{LJ}(r)$ is motivated by the existence of analytical solution of the free-space collisional problem, where the corresponding phase shifts are derived by means of a generalized effective range theory [39].

Hereafter, we assume that the length scales in our Hamiltonian are well separated, namely $\beta_6 \ll a_{\perp}$. Due to this separation, our configuration space has three distinct regions.

(i) In the asymptotic region $r \rightarrow \infty$ the interatomic potential V_{LJ} is negligible. Therefore, the wave function can be written as a linear combination of product states of plane waves in z -direction and a 2D harmonic oscillator state in the transversal ρ -direction. The relevant scattering information is then encapsulated in the

K^{1D} matrix. In addition, the total colliding energy E distributes over these two degrees of freedom according to $E = \frac{(a_{\perp}k)^2}{2} = 2n + 1 + \frac{(a_{\perp}q_n)^2}{2}$, where n refers to the oscillator modes, q_n denotes the momentum in the unconfined z -direction and k indicates the wave vector of the total energy.

(ii) Approaching the origin from the asymptotic region we pass through an intermediate regime ($\beta_6 \ll r \ll a_{\perp}$), where both the confining- and the interatomic- potential are negligible. Hence, the wave function in the corresponding region is simply the solution of the free particle Hamiltonian.

(iii) Finally, in the inner region ($r \sim \beta_6$), V_{LJ} becomes the by far dominant contribution and thus the two particles experience a free space collision with total energy $E = \frac{(a_{\perp}k)^2}{2}$, where the corresponding wave function can be written as a linear combination of the free space solutions. The impact of the V_{LJ} potential is then encompassed in the K^{3D} matrix.

The crucial assumption of length scale separation permits us to map the solutions from the inner region, where spherical symmetry is present and states are thus characterized by angular momentum eigenstates $|l\rangle$, to the states $|n\rangle$ in the asymptotic regime, where n denotes the n -th oscillator mode. We remark that in the inner and asymptotic region the azimuthal subgroup of the spherical symmetry group remains a symmetry of the Hamiltonian and therefore no mixing of different azimuthal states m occurs. Hence, we set $m = 0$ and omit it in the labeling of the states. The map accomplishing this local frame transformation from the spherical to the cylindrical solutions was used before [40, 41] and is generally given by

$$U_{\ell n} = \frac{\sqrt{2}(-1)^{d_0}}{a_{\perp}} \sqrt{\frac{2\ell + 1}{kq_n}} P_{\ell}\left(\frac{q_n}{k}\right), \quad (2)$$

where d_0 is either given by $\ell/2$ in the case of even partial waves, or, respectively by $(\ell + 1)/2$ in the case of odd partial waves and $P_{\ell}(\cdot)$ indicates the Legendre polynomial of ℓ -th degree. As mentioned above, Eq. (2) interrelates the wave functions of the asymptotic and the inner region. Consequently, the corresponding K matrices are connected according to the relation $K^{1D} = UK^{3D}U^T$ [18, 19, 28, 33], where the K^{3D} -Matrix is a diagonal matrix in the ℓ -wave representation with entries given by the tangent of the phase shifts.

Allowing K^{1D} and K^{3D} to be fully energy dependent, in the following we consider that the total colliding energy is well above the threshold of the transversal ground state and below the threshold to the first excited transversal mode. This implies that we assume only one open channel, namely the ground state of the harmonic oscillator, while all the excited states remain closed. However the part of the wave function which refers to the closed channels possess exponential divergences, and thus, results in an unphysical scattering process. To make the excited modes become evanescent, i.e.

impose the correct physical boundary conditions the multichannel quantum defect theory is used, which was first utilized in the context of CIRs in [18] and is in more detail generally discussed in [42], leaving us with a physical K -Matrix, given by

$$K_{oo}^{1D,phys} = K_{oo}^{1D} + iK_{oc}^{1D}(1 - iK_{cc}^{1D})^{-1}K_{co}^{1D}, \quad (3)$$

where K_{oo}^{1D} indicates the open-open channel transitions, K_{oc}^{1D} and K_{co}^{1D} refer to the K -matrices responsible for open-closed and closed-open channel transitions, respectively, while K_{cc}^{1D} denote the transitions between closed

channels. According to Eq. (3) the resonant processes are manifested as poles of the physical K^{1D} -matrix. Therefore, the roots of $\det(\mathbb{1} - iK_{cc}^{1D})$ correspond to the positions of closed channel bound states lying in the continuum of the open channel. This means that the corresponding resonant structure fulfills a Fano-Feshbach scenario.

Before addressing the question of how to relate the physical K -Matrix from Eq. (3) to the physical observables, let us for convenience introduce (c.f. App. A) the trace over the closed channels $\mathfrak{U}_{\ell\ell'}$ of $U_{\ell n}U_{\ell' n}$, for arbitrary angular momenta ℓ and ℓ' , by

$$\mathfrak{U}_{\ell\ell'}(\epsilon) = (-1)^{\frac{\ell+\ell'}{2}+\sigma} \sqrt{(2\ell+1)(2\ell'+1)} \sum_{\nu=|\ell-\ell'|}^{\ell+\ell'} \sum_{p=0}^{\nu} \frac{\Gamma(\ell, \ell', \nu, p)}{(\epsilon + \frac{1}{2})^{\frac{p+1}{2}}} \zeta(-\frac{p-1}{2}, n_o - \epsilon), \quad \text{with} \quad (4)$$

$$\Gamma(\ell, \ell', \nu, p) = i^{p-1} 2^{\nu-1} \begin{pmatrix} \ell & \ell' & \nu \\ 0 & 0 & 0 \end{pmatrix} (2\nu+1) \begin{pmatrix} \nu \\ p \end{pmatrix} \begin{pmatrix} \frac{\nu+p+1}{2} \\ \nu \end{pmatrix}$$

where n_o denotes the total number of open channels, which in the following is equal to 1. $\zeta(s, q)$ denotes the Hurwitz Zeta function, in the relation $\Gamma(\cdot)$ the terms which depend on ℓ, ℓ' and λ denote the Wigner $3J$ -symbols, while the last two expressions denote the binomial coefficients. ϵ is the dimensionless, channel normalized, total colliding energy, given by the relation $E = 2\omega_{\perp}(\epsilon + \frac{1}{2})$. This scale is chosen in such a way, that for $0 \leq \epsilon < 1$, the colliding energy varies between the thresholds of the ground- and the first excited transversal mode, respectively. It is clear from the definition of the trace, that $\mathfrak{U}_{\ell\ell'}$ describes the coupling of a partial wave ℓ to a ℓ' -wave after undergoing the virtual transitions in the closed channels n which are encapsulated in the Hurwitz Zeta functions.

Note that the elements of \mathfrak{U} can be used for different interatomic potentials, as long as harmonic confinement is considered and the separation of length scales is fulfilled. For example a minor generalization of them yields a convenient representation for the couplings to the closed channels with possible applications in the case of dipolar collisions.

The actual derivation of the physical K -Matrix essentially reduces to the inversion of the part containing the cc -channel contributions, i.e. $(\mathbb{1} - iK_{cc}^{1D})^{-1}$. Following the derivation in [19], we obtain a physical K -Matrix in the open channels, which reads

$$K_{oo}^{1D,phys} = \frac{1}{\det(\mathbb{1} - iK^{3D}\mathfrak{U})} \times \left(\Delta_{\ell}U_{\ell 0}^2 + \Delta_{\ell'}U_{\ell' 0}^2 - i\Delta_{\ell}\Delta_{\ell'}(\mathfrak{U}_{\ell'\ell'}U_{\ell 0}^2 + \mathfrak{U}_{\ell\ell}U_{\ell' 0}^2 - 2\mathfrak{U}_{\ell\ell'}U_{\ell 0}U_{\ell' 0}) \right), \quad (5)$$

where $K^{3D}\mathfrak{U}$ denotes the matrix product $\sum_{\lambda} K_{\ell\lambda}^{3D}\mathfrak{U}_{\lambda\ell'}$,

while $\Delta_{\ell} = \tan \delta_{\ell}$, whereas in turn δ_{ℓ} refers to the phase shift of the ℓ -th partial wave gathered in the interatomic collision via V_{LJ} . We remark, that Eq. (5) holds for arbitrary partial waves ℓ and ℓ' , under the assumption that either both are even or odd and at all energies within the continuum between the ground- and first excited channel. In particular we note, that in the case of $\Delta_{\ell'} = 0$, namely the single partial wave approximation, the formula reduces to

$$K_{oo}^{1D,phys} = \frac{\Delta_{\ell}U_{\ell 0}^2}{1 - i\Delta_{\ell}\mathfrak{U}_{\ell\ell}}, \quad (6)$$

which resembles for $\ell = 0$ and $\ell = 1$ the results found in [7] and [18], respectively.

III. K -MATRIX AND OBSERVABLES

In order to relate the physical K -Matrix to the relevant physical observables, different approaches were chosen in the past. One of the most common techniques to achieve this goal was to introduce an effective quasi 1D Hamiltonian to which the original Hamiltonian was mapped, where the short-range interaction is modeled by a bare delta function multiplied by a factor which is expressed in terms of the physical K -matrix [7, 19]. This technique was subsequently extended by the Bose-Fermi mapping to also include spin-polarized fermionic systems [18]. This procedure of mapping to an auxiliary Hamiltonian becomes cumbersome in the multi mode-regime, resulting in a family of effective Hamiltonians which are not uniquely defined.

To avoid this difficulty we present an alternative method which by construction is valid for an arbitrary

number of open channels, applies equally well to distinguishable and indistinguishable particles and provides the full scattering wave function. To obtain the full solution to the scattering problem, we essentially have to find a connection of the 1D scattering amplitude f_{1D} and the physical K -Matrix $K_{oo}^{1D,phys}$. This is done by exploiting the relation $S = \mathbb{1} + \left(\frac{ik}{2\pi}\right)^{\frac{d-1}{2}} \hat{f}$, [43] where S denotes the scattering matrix of the system and \hat{f} is an integral operator [44] averaging the scattering amplitude over the solid angle. It relates the scattering amplitude and the scattering matrix in arbitrary dimensions d . For our purpose we consider the special case $d = 1$ and obtain, by evaluating the integral to be two times the scattering amplitude, an expression for the 1D scattering matrix, given by

$$S_{1D} = \mathbb{1} + 2f_{1D}, \quad (7)$$

which, in particular differs from the standard textbook result for the 3D relation by the absence of an additional momentum dependence compensating for the physical dimension of the 3D scattering amplitude. Using now the Cayley transform $S = (1 + iK)(1 - iK)^{-1}$ we obtain the 1D scattering amplitude in terms of the physical $K_{oo}^{1D,phys}$

$$f_{1D} = \frac{iK_{oo}^{1D,phys}}{1 - iK_{oo}^{1D,phys}}, \quad (8)$$

and correspondingly the well-known expression for the transmission amplitude

$$T = |1 + f_{1D}|^2 = \frac{1}{1 + (K_{oo}^{1D,phys})^2} \quad (9)$$

Note that Eqs. (8) and (9) hold regardless of the particle exchange symmetry. The bosonic or fermionic character of the particles is already embedded in the $K_{oo}^{1D,phys}$ matrix. Furthermore, we remark that this derivation is not restricted to quasi-1D Hamiltonians and can be equally applied to Hamiltonians of arbitrary dimensions connecting the relevant physical K matrix with the corresponding scattering amplitudes and cross-sections.

In addition, let us give some general remarks on Eq. (9) concerning the two significant values the transmission coefficient can take, namely $T = 0$ which especially addresses the CIR, and, $T = 1$ corresponding to total transparency characterizing in particular the absence of a back-scattering process. As the general form of the transmission coefficient is given by Eq. (9), we immediately observe, that the zeros of the transmission are in one-to-one correspondence with a diverging physical K -Matrix, while the unit values appear for a vanishing $K_{oo}^{1D,phys}$. The inspection of Eqs. (5) and (6) shows, as the physical K -Matrix is in both cases clearly separated in numerator and denominator, that a zero value and divergence of the physical K -Matrix can only be obtained by a root of the numerator and denominator, respectively. The case of a diverging numerator can be excluded since the elements

of the local frame transformation $U_{\ell 0}$ and the particular $\mathfrak{U}_{\ell\ell'}$'s behave regular within the range of considered energies. In the present investigation we exclude the threshold energy $\epsilon = 1$ of the first excited channel, since over there the elements of $\mathfrak{U}_{\ell\ell}(\epsilon)$ are in general singular and thus lead to threshold singularities [44, 45], arising due to the fact that at the channel thresholds the S -Matrix of the system abruptly changes its dimension since additional transitions between the open channels become available.

IV. RESULTS AND DISCUSSION

A. Universal properties of ℓ -wave CIRs

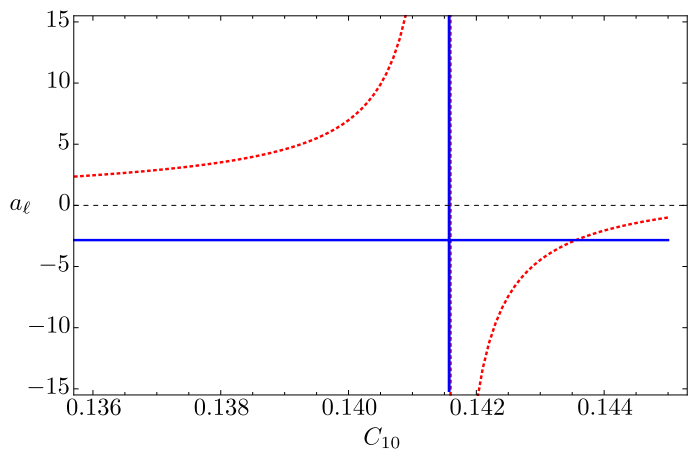


FIG. 1. (Color online) The s -wave scattering length a_0 (red dashed line) and the g -wave scattering length a_4 (blue solid line) are shown versus the C_{10} parameter. It is observed, that both scattering lengths are diverging at the same values of C_{10} meaning that the s - and g -wave bound and quasi-bound states appear simultaneously at the threshold.

In the following we will focus on the universal properties of the ℓ -wave CIRs. Since our main concern is the description of neutral alkaline atomic collisions in the presence of a waveguide the following analysis depends on the van der Waals tail of the interatomic interactions. From the perspective of free-space collisions Gao [46] developed an angular insensitive quantum defect theory focusing on pair collisions under the influence of a van der Waals potential tail. Investigating the universal aspects of such collisional systems it was shown that the resonant structure of different ℓ partial waves possesses a periodic character with respect to the angular momentum. More specifically, it was shown that when an ℓ -wave (quasi-)bound state crosses the threshold simultaneously an $\ell + 4$ -wave (quasi-)bound state crosses it as well. This remarkable property is demonstrated in Fig. 1 where in a transparent way we show that s - (red dashed line) and g -wave (blue solid line) scattering lengths are diverging simultaneously. The same holds for p - and h -wave, d -

and i -wave, f - and k -wave, respectively.

Considering the same set up within a waveguide the transversal confinement results into a coupling among all the partial waves. In this case a particular CIR possesses a specific ℓ -wave character when the corresponding partial wave dominates over the remainder or in other words an ℓ -wave CIR occurs in the vicinity of an ℓ wave free-space resonance. Therefore, the interplay of the confinement with the $\ell + 4$ periodicity of the van der Waals potential yields four universal ℓ -wave CIRs, namely s , p , d , f , overwhelming the corresponding contributions of $\ell + 4$ partial waves. This simply means that there are two ℓ -wave CIRs for bosonic collisions and two more for the fermionic ones.

As Gao's findings on the $\ell + 4$ periodicity crucially depend on the assumption that all (quasi-)bound states must be close to the threshold of the interatomic potential, we express the energy scale associated with this potential ϵ_{sh} , introduced in [46], in terms of the confinement length scale, yielding:

$$\epsilon_{\text{sh}} = \frac{(\epsilon + 1/2)\hbar}{4\mu} \left(\frac{\beta_6}{a_{\perp}}\right)^2, \quad (10)$$

which shows, that the length scale separation ($\beta_6 \ll a_{\perp}$) also separates the energy scale of the waveguide, given by ϵ and the interatomic energy scale, given by ϵ_{sh} . Thus, we can safely assume to be in the regime nearby the threshold of the interatomic potential while still being allowed to consider colliding energies $\epsilon \sim 1$, and thus be well above the threshold of the transversal ground state.

Another universal aspect of the ℓ -wave CIRs is the following: when a s or a p -wave CIR occurs, their corresponding couplings to d or f partial waves, respectively, can be neglected. This is permitted since in general d and f -wave scattering lengths are practically zero in the vicinity of s - and a p -wave free space resonances, respectively. Contrary to the previous case, when a d - or an f -wave CIR occurs their corresponding couplings to the s - or p -wave can not be neglected. This occurs due to the fact that for energies ranging in the interval $\epsilon \in [0, 1]$, in the vicinity of a d -wave CIR the s -wave scattering length has the value $a_{0_{bg}} \approx 2\pi/(\Gamma(1/4)^2)\beta_6 \approx 0.48 \beta_6$ and, similarly, in the vicinity of an f -wave CIR the p -wave scattering length has the value $a_{1_{bg}} \approx -0.45 \beta_6$, where the corresponding analytical values are taken from [46].

B. s - and p -wave energy dependent CIRs

For now, we turn our attention to the simplest cases where CIRs occur, i.e. s - and p -wave interactions for bosons and spin-polarized fermions, respectively. In this case, the resonant collisions within the waveguide result in s - and p -wave CIRs. A fundamental property of this particular type of CIR is that they are solely characterized by one partial wave and hence are well described within the single partial wave approach. This is due to

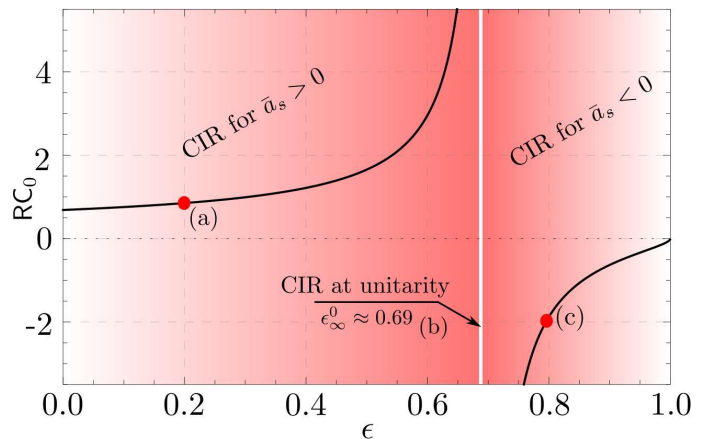


FIG. 2. (Color online) The coefficient $RC_{\ell}(\epsilon)$ (black solid lines) from Eq.(12) versus the dimensionless energy ϵ is shown for the case of $\ell = 0$. (a) to (c) refer to the values of energy for which the transmission coefficient T is shown versus the scattering length in Fig. 4. The shading indicates the magnitude of the scaled scattering length (\bar{a}_0) that has to be met fulfilling the equality of the resonance condition Eq. (11), while the white line represents the pole in the resonance condition after which the CIR occurs with a negative sign in scattering length.

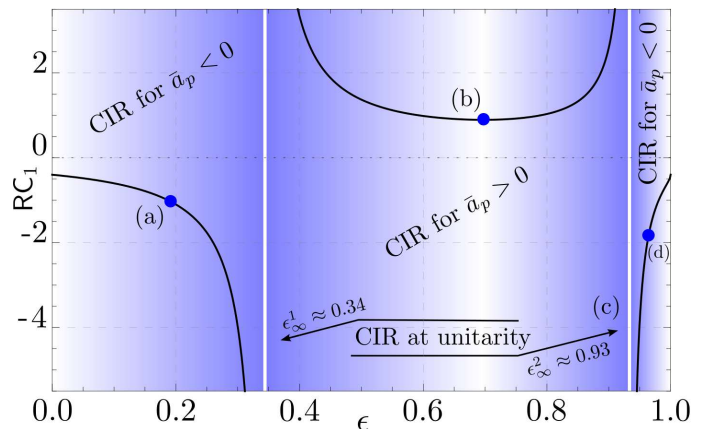


FIG. 3. (Color online) Analogous to Fig. 2, here $RC_1(\epsilon)$ is shown. The panels (a) to (d) correspond to the values of energy for which the transmission coefficient T is shown in Fig. 5. Note, that this time the resonance condition has two poles resulting in a twofold sign change in the scattering length.

the fact that in the vicinity of these CIRs all higher partial waves have practically a vanishing scattering length, namely $a_{\ell} \approx 0$.

In general, in the single partial wave picture, we obtain, by solving $\det(1 - iK_{cc}) = 0$ for the scattering length the *resonance condition*

$$\bar{a}_{\ell}(\epsilon) = RC_{\ell}(\epsilon) \quad (11)$$

for a specific ℓ -wave CIR, where $\text{RC}_\ell(\epsilon)$ is given by:

$$\text{RC}_\ell(\epsilon) = \frac{-1}{2\sqrt{\epsilon + 1/2}} \times {}^{2\ell+1}\sqrt{\frac{1}{i\mathfrak{U}_{\ell\ell}(\epsilon)}} \quad (12)$$

The scaled scattering length $\bar{a}_\ell(\epsilon) = a_\ell(\epsilon)/a_\perp$, introduced above, is defined as the energy dependent ℓ -wave free space scattering length divided by a_\perp , whereas in turn, the energy dependent scattering length is as usual given by: $a_\ell^{2\ell+1} = -\tan\delta_\ell/k^{2\ell+1}$. For $\ell = 0$ and $\epsilon = 0$, this relation reduces to Olshanii's result [7], while the corresponding case of $\epsilon = 0$ and $\ell = 1$ describes the p -wave CIR found by Granger *et al.* in [18].

For the case of s -wave CIRs, we show in Fig. 2 the coefficients RC_0 versus the dimensionless energy ϵ depicted as black solid lines, while the red shading illustrates the magnitude, which $\bar{a}_0(\epsilon)$ has to have at a certain energy in order to form a CIR. Over there we readily read off the familiar value of $\bar{a}_0(0) = -1/\zeta(1/2) \approx 0.68$ at $\epsilon = 0$. Now, as we move on to higher energies we see that the scaled scattering length also has to increase in order to become resonant until, at an energy $\epsilon_\infty^0 \approx 0.69$, the resonance coefficient RC_0 becomes infinite and thus the (scaled) scattering length must be close to unitarity in order to satisfy Eq. (11).

Similarly to the s -wave CIRs, the corresponding coefficients RC_1 for the p -wave CIRs are shown by the black solid line in Fig. 3, while the blue shading this time corresponds to the magnitude of \bar{a}_1 in order to meet the resonance condition Eq. (11). We observe that here a similar behavior is present. This time departing at $\epsilon = 0$ with a small negative value, the resonance coefficients monotonically decreases until they reach $-\infty$ at $\epsilon_\infty^1 \approx 0.34$. In that sense, the main difference between the resonance conditions for $\ell = 1$ and $\ell = 0$ is, that the coefficient RC_ℓ for p -waves has two poles, whereas the bosonic counterpart only exhibits one pole, respectively. However, common to both coefficients is the fact, that the poles are of odd order, or, equivalently, are related to sign changes in the resonance condition, implying that for both partial waves the CIR can occur for both signs of the scaled scattering length. To be more specific, for $\ell = 0$ the CIR can appear for energies larger ϵ_∞^0 if and only if $\bar{a}_0 < 0$, while for $\epsilon < \epsilon_\infty^0$, the CIR can occur only for values of \bar{a}_0 being positive. The fermionic case of $\ell = 1$ allows for positive (CIR) values of \bar{a}_1 if and only if the energy lies in the interval $\epsilon_\infty^1 < \epsilon < \epsilon_\infty^2 \approx 0.93$, while CIRs with a negative value of \bar{a}_1 can occur for the remaining energies, namely $\epsilon < \epsilon_\infty^1$ and $\epsilon > \epsilon_\infty^2$. This is in particular illustrated in Figs. 4 (a) and (c) for bosons and Figs. 5 (a),(b) and (d) for fermions, respectively. There, the transmission coefficient T is shown versus the corresponding scaled scattering length \bar{a}_ℓ at different energies, which are also labeled by the corresponding letters in Figs. 2 and 3, respectively. In these transmission spectra the CIRs, identified by a vanishing transmission, appear at the values given according to Eq. (12). We also observe, that the values of $T = 1$, i.e. the total transparency, is always located at

$\bar{a}_\ell = 0$, as it is expected by our earlier discussion in the last paragraph of Sec. III on the vanishing of the physical K -Matrix. In the case of a single partial wave a vanishing numerator of the K -Matrix can only be achieved by a vanishing scattering length, i.e. by the absence of the free-space interactions.

Note the black dots in Figs. 4 and 5, which indicate *ab initio* numerical simulations based on [47] where we solve directly the Hamiltonian in Eq. (1). The numerical simulations are in excellent agreement with the corresponding analytical calculations, namely red and blue solid lines in Figs. 4 and 5, respectively. As seen in Figs. 4 (b) and 5 (c) the situation changes, when considering the transmission coefficient at the particular values of energy ϵ_∞^i , where $\text{RC}_\ell(\epsilon)$ diverges. There, in particular we recognize, that the asymmetric Fano line-shape, typical for a Fano-Feshbach resonance, is absent and instead a symmetric Lorentzian shape of the transmission coefficient is observed. An explanation of this effect is given by the fact, that the elements of $\mathfrak{U}_{\ell\ell'}(\epsilon)$ by construction describe the coupling of the bound states supported by all closed channels to the open via a particular ℓ -wave. Therefore, at the particular values ϵ_∞^i , $i = 1, 2, 3$, the corresponding elements vanish, yielding the decoupling of the closed channel bound states from the continuum of the open one. In other words, this means that the pair of atoms experience an *effective* free-space collision within the waveguide, where resonant scattering occurs for $\bar{a}_0 = \infty$ as in free-space.

One way to describe the transition between the regime where a CIR is present and its absence is most conveniently done by introducing the Fano q -parameter [48], which is originally defined as the ratio between the transition probabilities to the discrete state and to the continuum. Following this nomenclature, the symmetric line-shape is obtained when the transition to the continuum tends to zero, namely the coupling between closed channel bound state and the open channel continuum vanishes, and hence q diverges. For a general ℓ -wave confinement-induced processes, we define the ℓ -dependent q -parameter q_ℓ to be:

$$q_\ell := -(\text{RC}_\ell)^{2\ell+1} \quad (13)$$

Using this parametrization, the transmission coefficient reads

$$T = \frac{(\bar{a}_\ell^{2\ell+1} - q_\ell)^2}{(\bar{a}_\ell^{2\ell+1} - q_\ell)^2 + (q_\ell \Delta_\ell U_{\ell 0}^2)^2}. \quad (14)$$

Taking now the limit $\epsilon \rightarrow \epsilon_\infty^i$, the q -parameter q_ℓ diverges and we end up with:

$$T_\infty = \frac{\epsilon_\infty^0}{\epsilon_\infty^0 + (\bar{a}_0)^2}, \quad (15)$$

as the expression for the transmission coefficient in the case of $\ell = 0$, describing the Lorentzian line shape which

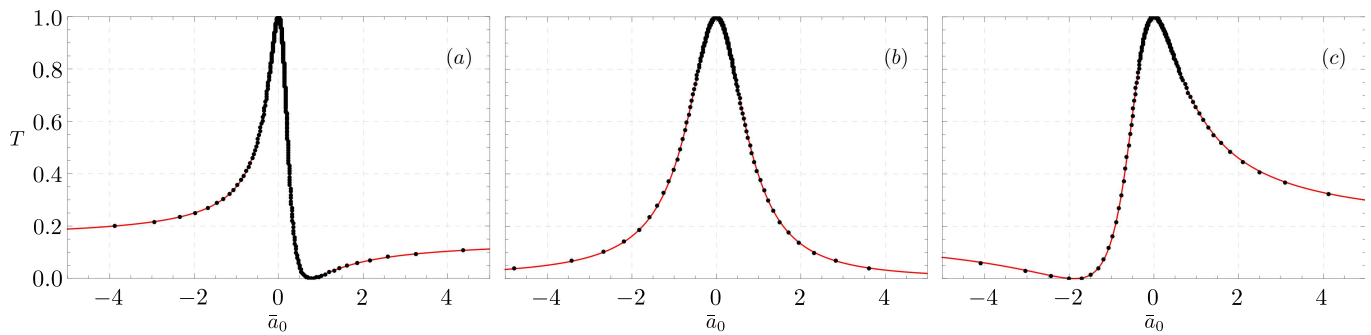


FIG. 4. The analytically calculated transmission coefficient (solid lines) is plotted versus the scaled s -wave scattering length \bar{a}_0 for energies $\epsilon = 0.1, 0.69, 0.8$ from left to right. Corresponding to the energy values indicated by the red dots in Fig. 2. The black dots indicate numerical values for the transmission coefficient included for comparison.

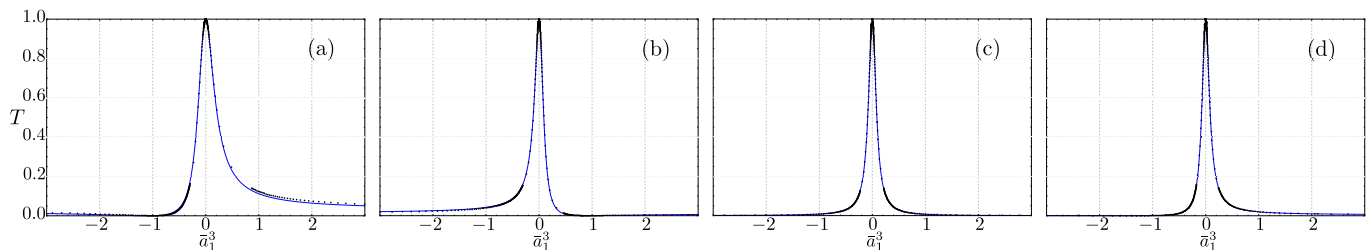


FIG. 5. Same as Fig. 4, but this time for $\ell = 1$ and energies $\epsilon = 0.2, 0.7, 0.93, 0.97$, from left to right, as indicated in Fig. 3.

is solely parameterized in terms of the scaled scattering length \bar{a}_0 . Similarly, for the case of $\ell = 1$ we obtain:

$$T_\infty = \frac{(\epsilon_\infty^j)^{-1}}{(\epsilon_\infty^j)^{-1} + 144(\bar{a}_1^3)^2}, \quad (16)$$

where, in Eq. (16), ϵ_∞^j for $j = 1, 2$ refer to the energies at the poles in the coefficients RC_1 . Again, this transmission coefficient is parameterized by the scaled scattering length \bar{a}_1 .

As we mentioned above at energies $\epsilon = \epsilon_\infty^i$ the resonant collisions occur at $\bar{a}_\ell \rightarrow \infty$ yielding transmission blockade, i.e. $T = 0$. In order to firmly address this point we consider that the corresponding scattering lengths are deeply in the unitarity regime. Then for a single partial wave ℓ the general form of the transmission coefficient T given in Eq. (9) for scattering lengths at unitarity reduces to $T_{\text{unitarity}}$ according to the following relation:

$$T_{\text{unitarity}} = \lim_{\Delta_\ell \rightarrow \infty} T = \frac{\mathfrak{U}_{\ell\ell}^2(\epsilon)}{\mathfrak{U}_{\ell\ell}^2(\epsilon) - U_{\ell 0}^4(\epsilon)}, \quad (17)$$

where we refer to the Appendix A for further details on \mathfrak{U} . Eq. (17) is depicted in Fig. 6 both for s -wave (red line) and p -wave (blue dashed line) cases, where we plot the transmission coefficient $T_{\text{unitarity}}$ on a logarithmic scale as a function of energy ϵ . As expected we observe that indeed the transmission $T_{\text{unitarity}}$ becomes zero at the energy values ϵ_∞^0 for the s -wave case and $\epsilon_\infty^1, \epsilon_\infty^2$ for the p -wave case.

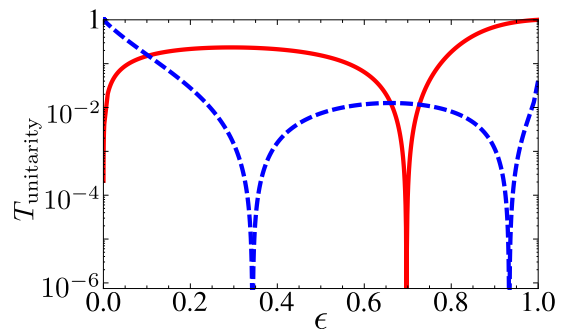


FIG. 6. (Color online) The transmission coefficient $T_{\text{unitarity}}$ at unitarity is shown versus the channel normalized energy ϵ for $\ell = 0$ and $\ell = 1$, solid and dashed curve, respectively. Note that the minima indeed appear at ϵ_∞^0 for $\ell = 0$ and at ϵ_∞^1 and ϵ_∞^2 for $\ell = 1$, as these denote the location of the poles in Figs. 2 and 3, respectively.

C. d - and f -wave energy dependent CIRs

Let us now discuss the case of d - and f -wave CIRs where we will solely focus on the universal properties of the extrema of the corresponding transmission coefficients. Unlikely to the case of s - and p -wave CIRs, d - and f -wave CIRs are strongly affected by the presence of s - and p -partial waves, respectively. This occurs since in the vicinity of these CIRs the s - and p -wave scattering lengths retain a non-vanishing value. Therefore, the single partial wave approach is not valid anymore partic-

ularly for $T \approx 1$.

First we consider the case $T = 0$. Analogous to the case of a single partial wave, the *resonance condition* $\bar{a}_{\ell'} = \text{RC}_{\ell',\ell}(\epsilon)$ in the presence of two partial waves ℓ and ℓ' is obtained by solving the determinant from Eq.(5) for the corresponding scattering length, yielding the following expression

$$\text{RC}_{\ell',\ell}(\epsilon) = \frac{-1}{2\sqrt{\epsilon + 1/2}} \times {}^{2\ell'+1}\sqrt{\frac{1}{i(\mathfrak{U}_{\ell'\ell'} - \alpha_{\ell}\mathfrak{U}_{\ell\ell'}^2)}}, \quad (18)$$

where $\alpha_{\ell} = i\Delta_{\ell}/(1 - i\Delta_{\ell}\mathfrak{U}_{\ell\ell})$ represents the coupling strength of the ℓ' -wave to the ℓ -wave and essentially describes how the free space process is affected by the closed channels, which can be seen by comparing α_{ℓ} with Eq. (6). Equation (18) nicely shows, how the corresponding coefficients from Eq. (12) are altered by the presence of a second partial wave. Also note, that in the single partial ℓ' -wave approximation, we have $\Delta_{\ell} = 0$, and hence $\alpha_{\ell} = 0$, Eq. (18) reduces to Eq. (12).

As mentioned before, the ℓ -wave character is addressed to a CIR if and only if the corresponding partial wave dominates over all the others. Therefore, for the particular case of $T = 0$, d and f -wave CIRs occur when the corresponding scattering lengths dominate. Hence, the background scattering lengths, namely s and p -wave can be regarded as minor corrections to the positions of d - and f -wave CIRs.

Now, similar to the case of $T = 0$ we investigate the solutions to the constraint $T = 1$, i.e. total transparency, since the numerator of the physical K -Matrix for coupled partial waves, given in Eq. (5), contains non-trivial relations between the different partial waves, as well as couplings to the closed channels. Hence, analogous to the resonance condition of Eq. (11), we obtain the *transparency condition* for a ℓ' -wave dominated process, given by

$$\bar{a}_{\ell'}(\epsilon) = \text{TC}_{\ell',\ell}(\epsilon), \quad (19)$$

where the coefficients $\text{TC}_{\ell',\ell}(\epsilon)$ are

$$\text{TC}_{\ell',\ell}(\epsilon) = \frac{1}{2\sqrt{\epsilon + 1/2}} \times {}^{2\ell'+1}\sqrt{\frac{\Delta_{\ell}U_{\ell 0}^2}{U_{\ell' 0}^2 - i\Delta_{\ell}(\mathfrak{U}_{\ell'\ell'}U_{\ell 0}^2 + \mathfrak{U}_{\ell\ell}U_{\ell' 0}^2 - 2\mathfrak{U}_{\ell\ell'}U_{\ell 0}U_{\ell' 0})}}, \quad (20)$$

However, in the case of total transparency, we observe from Eq. (20) that the value of $\bar{a}_{\ell'}$ for which T becomes unity strongly depends on the corresponding background scattering length as well as on the colliding energy ϵ . Also note, that in the case of a single partial wave, e.g. $\Delta_{\ell} = 0$, the RHS of Eq. (20) vanishes identically and we are left with the conclusion from Sec. IV B, that total transparency can occur only for $\bar{a}_{\ell} = 0$. Hence, contrary to s - and p -wave total transparency, here, in the case of coupled partial waves, the occurrence of the total transparency is the immediate result of destructive interference between $s - d$ and $p - f$ partial waves for bosons or fermions, respectively. Therefore this feature of CIR corresponds to the bosonic and fermionic *dual* CIR which has been discussed in Ref. [17] for distinguishable particles.

Figures 7, 8 and 9 present a convenient visualization of the energy dependence of the transmission extrema for s -, p -, d - and f -wave (dual) CIRs. This representation is achieved by stereographically projecting on a cylinder the geometrical topos, i.e. the trajectory, of the corresponding coefficients $\text{RC}_{\ell',\ell}$ and $\text{TC}_{\ell',\ell}$ for $T = 0$ and $T = 1$, respectively. The basis of the cylinder is formed by mapping the complete range of values of the scaled scattering length \bar{a}_{ℓ} on a circle. This particularly allows us to illustrate the values $\bar{a}_{\ell} = 0$ and $\bar{a}_{\ell} = \pm\infty$ as two anti-diametric points of the circle. In addition perpendicularly to the plane of the circle we add the axis of the energy ϵ .

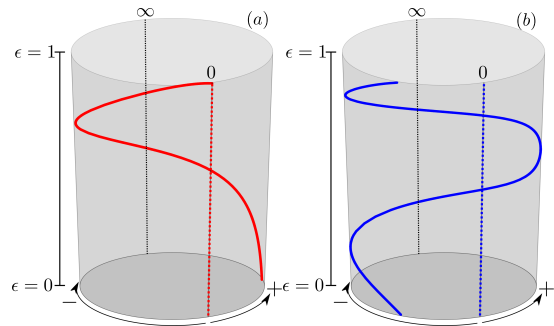


FIG. 7. (Color online) The solid lines in panels (a) and (b) depict $\text{RC}_0(\epsilon)$ and $\text{RC}_1(\epsilon)$, respectively, while both dashed lines show the condition for $T=1$, i.e. total transparency.

More specifically, the panels (a) and (b) of Fig. 7 corresponds to the cases of s and p -wave CIRs respectively. In both panels we observe that the resonance trajectories (dashed lines) for $T = 1$ are completely straight lines on the corresponding cylindrical surfaces demonstrating in this manner that they do not depend on energy. On the other hand the resonance trajectories for $T = 0$ (solid lines) exhibit a more intricate dependence on the energy. The resonance trajectories spiral upwards as the energy is increased illustrating in a transparent way the sensitivity of the position of s and p -wave CIRs which alter via the total colliding energy yielding thus CIRs even for

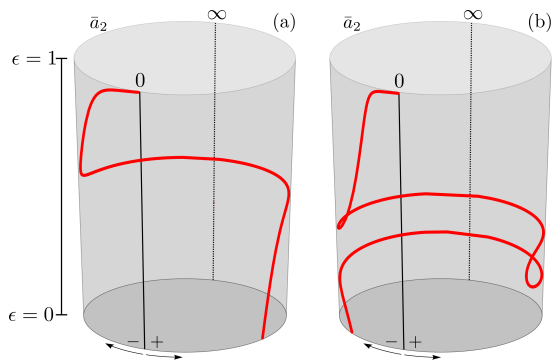


FIG. 8. (Color online) For the case of d -wave CIR, panel (a) shows the resonance coefficients $RC_{2,0}(\epsilon)$ versus the total colliding energy ϵ . (b) shows, also versus ϵ , the transparency coefficients $TC_{2,0}(\epsilon)$, which is seen to depend strongly on energy.

negative scattering lengths. This change in the sign occurs when the position of the corresponding CIRs cross the infinity point, namely $\bar{a}_\ell = \pm\infty$. In addition in Fig. 7 (b) we observe that the energy dependence yields a double change on the sign of the p -wave scattering length as it was already shown in Figs. 3 and 5.

Figs. 8 and 9 corresponds to d - and f -wave CIRs, respectively. More specifically, panel (a) in Figs. 8 and 9 refer to the cases of d - and f -wave CIRs, respectively. The resonance trajectories for $T = 0$ are denoted by red and blue solid lines for d - and f -wave CIRs, respectively. We observe that both cases exhibit similar behavior as in the corresponding cases of s - and p -wave CIRs. This occurs since the corresponding resonance conditions (Eqs. (12) and (18)) contain the same zeta function pieces attributing therefore similar behavior to s - and d -wave CIRs or p - and f -wave CIRs.

Furthermore, we observe in panel (b) of Fig. 8 that the resonance trajectory for $T = 1$ strongly depends on energy yielding thus the following behavior: The position

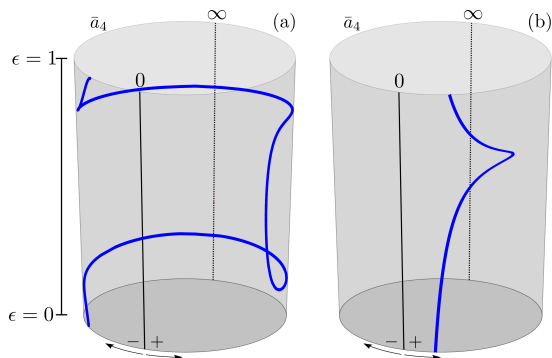


FIG. 9. (Color online) For the case of f -wave CIR, analogous to Fig. 8. Panel (a) depicts $RC_{3,1}(\epsilon)$ and panel (b) $TC_{3,1}(\epsilon)$. Contrary to the bosonic counterpart shown in Fig. 8 we observe from panel (b), that there is now f -wave dual CIR for negative values of \bar{a}_4 .

of $T = 1$ spirals up initially counterclockwise with respect to the resonance trajectory $T = 0$ and evidently the corresponding scattering length is changing sign across the point $\bar{a}_\ell = \infty$ in order to fulfill the condition Eq. (19). Comparing this observation with the corresponding fermionic case, i.e. the behavior of $TC_{3,1}(\epsilon)$ which is shown in panel (b) of Fig. 9, we find that the dependence on energy is not as intricate as it is for the corresponding bosonic coefficient $TC_{2,0}(\epsilon)$. This behavior is an immediate result of the weak interference of p and f waves. Additionally, we observe that there is no f -wave dual CIR for negative values of \bar{a}_4 .

As we mentioned above, the trajectories of Figs. 7 to 9 for $T = 0$ and for $T = 1$ occur from the roots of the denominator and nominator of the physical K -matrix, respectively. Therefore, intersections between the $T = 0$ - and $T = 1$ -trajectories are prohibited since this would result in an indeterminate physical K -matrix. Or, in terms of physical behavior, this would yield a scenario where the transmission T would be simultaneously zero and unity at the corresponding scattering length and energy. However, we remark that the trajectories $T = 0$ and $T = 1$ might approach each other at some particular values of the scaled scattering lengths and energies and exhibit in this manner a transmission profile where T abruptly changes from total transparency to total reflection. Hence, close to these *exceptional* values the full physical K -matrix has to be employed and not its parts, namely the nominator and the denominator yielding thus trajectories which do not possess crossings.

D. Confinement-induced resonances and closed channel bound states

In this subsection we address the physical interpretation of the energy dependent ℓ -wave CIRs. As we mentioned above this particular type of resonances fulfill a Fano-Feshbach scenario. Therefore, a detailed analysis based on the bound eigenspectrum of the closed channels will allow us to rigorously show that indeed an ℓ -wave CIR can occur even when the two-body interactions are not deep enough to sustain a (quasi-) bound state thereby going beyond previous studies [8].

In the following we will calculate the bound state eigenenergies via the roots of $\det(1 - iK_{cc})$, where the K_{cc} matrix is fully energy dependent [42]. Moreover, we remark that $\det(1 - iK_{cc})$ contains only the closed channel bound states and not their couplings to the continuum of the open channel. This means that Fig. 10 illustrates the bare bound states of the closed channels and not the dressed ones. Specifically, Fig. 10 (a) depicts the bound states of s - (red solid line) and p -wave CIRs (blue dashed line) as a function of their corresponding inverse scaled scattering lengths, namely \bar{a}_ℓ^{-1} , where the horizontal dashed line indicates the amount of the total colliding energy ϵ_{tot} .

The s -wave case, i.e. $\ell = 0$, is in accordance with

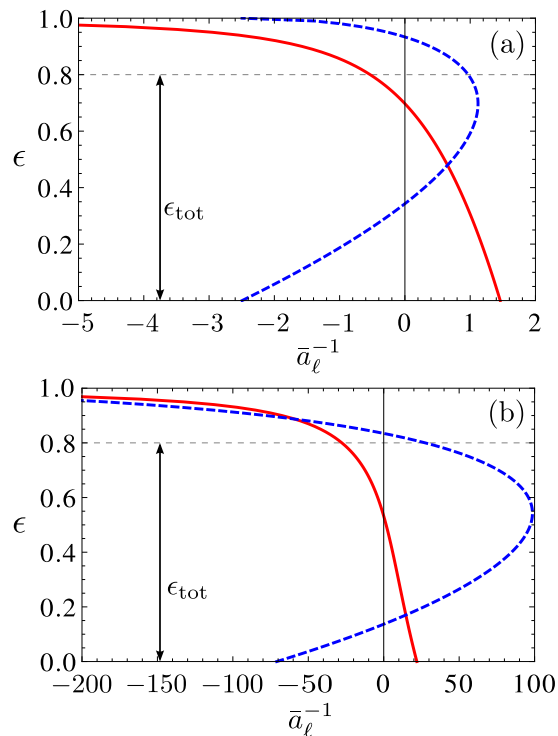


FIG. 10. (Color online) The eigenenergies of the closed channel bound states of the ℓ -wave CIRs as a function of the corresponding inverse scattering length, namely \bar{a}_ℓ^{-1} . (a) shows the bound states of s - (red solid line) and p -wave (blue dashed line) CIRs and (b) depicts the bound-states of d - (red solid line) and f -wave CIRs (blue dashed line). The horizontal dashed line illustrates the total colliding energy ϵ_{tot} .

the corresponding results of [8]. In particular we observe that for $\epsilon_{\text{tot}} = 0$ the corresponding bound state crosses the threshold of the transversal ground state at $a_\perp/a_0 = 1.46\dots$, as expected. Increasing the total colliding energy ϵ_{tot} , i.e. moving away from the threshold of the open channel we observe that the intersection of the horizontal dashed line with the red solid one changes its location continuously towards smaller values of a_\perp/a_0 until it crosses the zero which occurs at $\epsilon_{\text{tot}} = \epsilon_\infty^0$ as it was mentioned before (see Fig. 2) and from that colliding energy on, the incoming wave can become resonant with the closed channel bound state only for negative scattering lengths until the threshold to the first excited channel is reached from below. Similarly in Fig.10 (b), this general behavior is also observed for the bound state of the d -wave CIRs indicated by the red solid line.

On the other hand, the bound states of the odd partial waves behave differently. As already observed in the respective panel (b) of Figs. 8 and 9, there are two colliding energies for which the corresponding trajectories for $T = 0$ are crossing the value $\bar{a}_\ell = \infty$ for two different colliding energies. This behavior is clearly demonstrated in Fig 10 (a) and (b) where we observe that the corresponding blue dashed lines cross twice the value $\bar{a}_\ell^{-1} = 0$, implying, a twofold change of sign in the scaled scattering

length with increasing total colliding energy ϵ_{tot} to ensure resonant scattering within the waveguide geometry. To conclude, Fig. 10 shows in a transparent way that *all* ℓ -wave CIRs render the existence of a closed channel bound state even though the underlying two-body potential may not support a (quasi-) bound state.

V. SUMMARY AND CONCLUSIONS

We have investigated the two-body scattering of bosons and spin-polarized fermions in a harmonic waveguide, taking into account the coupling of different partial waves due to the confinement, as well as the energy dependence of the collisional processes. Furthermore, we employ the framework of the K -matrix approach presented in [18, 19, 28, 33] which we combined with the free-space collisional theoretical framework of Gao [39, 46, 49]. This permits us to obtain fully analytical results including adequate two-body interatomic interactions which possess a van der Waals tail.

Throughout this work the only assumption that we considered is that the length scale associated with the interatomic potential is smaller than the oscillator length a_\perp , implying two regions of different symmetry, i.e. spherical close to the center and cylindrical for large relative distances. In addition, we present analytical formulas which provide a connection of the physical K -matrix with all the relevant scattering observables, in particular to the scattering amplitudes, and matrices. This connection provides a general form and can be applied to different confining potentials or an arbitrary number of open channels regardless if the collisional partners are constituted of identical or distinguishable particles.

In the present set up of identical particle collisions within a quasi-1D waveguide geometry we have demonstrated the universal aspects of ℓ -wave CIRs concluding that atomic collisions render four types of CIRs, where two of them are attributed to bosons and the other two to spin polarised fermions. We show that this property arises due to the interplay of the van der Waals potential with the transversal confinement. In addition, we have investigated the energy dependence of ℓ -wave CIRs showing that all of them possess always a closed channel bound state even if the two-body potential is not deep enough to support a weakly or quasi-bound state. Therefore the fact that the position of the CIRs are extremely sensitive to the total colliding energy regardless of the dimensionality of the confining potential might be an indicator for the experimental discrepancies on the sign of the position of a quasi-2D CIR [11, 13]. Moreover, we observe that at some particular colliding energies the closed channel bound states decouple from the continuum of the open channel resulting thus into an effective free-space collision within the waveguide. Particularly in the case of d and f -wave collisions we observed the dual CIR, i.e. total transparency, for indistinguishable particles which is due to the interference of different partial waves and

exhibits a strong energy dependence.

Appendix A: Derivation of the \mathfrak{U} -Matrix

Starting with the *Local Frame Transformation*:

$$U_{\ell n} = \frac{\sqrt{2}(-1)^{d_0}}{a_{\perp}} \sqrt{\frac{2\ell+1}{kq_n}} P_{\ell}\left(\frac{q_n}{k}\right), \quad (\text{A1})$$

where d_0 abbreviates $\ell/2$ or $(\ell+1)/2$ for even, respectively odd partial waves and $P_{\ell}(\cdot)$ denotes the ℓ -th Legendre polynomial, the focus of this subsection is the computation of the coupling of a state $|\ell\rangle$ to a state $|\ell'\rangle$ after undergoing a transition through the collective bound state from the closed channels, i.e. we want to calculate $\sum_{n=n_o}^{\infty} \langle \ell|n\rangle \langle n|\ell'\rangle$, which is explicitly given by the sum over the appropriate locale frame transformations, i.e.:

$$\mathfrak{U}_{\ell\ell'} := \sum_{n=n_o}^{\infty} U_{\ell n} U_{\ell' n}, \quad (\text{A2})$$

where n_o denotes the number of open channels. We note that n_o should not be confused with the corresponding oscillator quantum number, i.e. for a value of $n_o = N$, the highest accessible oscillator mode is $|N-1\rangle$. Explicitly writing Eq. (A2) yields

$$\begin{aligned} \sum_{n=n_o}^{\infty} U_{\ell n} U_{\ell' n} &= \frac{2(-1)^{\frac{\ell+\ell'}{2}+\sigma}}{a_{\perp}^2 k} \sqrt{(2\ell+1)(2\ell'+1)} \times \\ &\times \sum_{n=n_o}^{\infty} \frac{P_{\ell}\left(\frac{q_n}{k}\right) P_{\ell'}\left(\frac{q_n}{k}\right)}{q_n}, \end{aligned} \quad (\text{A3})$$

where σ is 0, 1 in the case of even, odd partial waves ℓ and ℓ' .

A common expansion for the product of two Legendre

Polynomials given by

$$\begin{aligned} P_{\ell}(x)P_{\ell'}(x) &= \\ &= \sum_{\nu=|\ell-\ell'|}^{\ell+\ell'} \sum_{p=0}^{\nu} 2^{\nu} \begin{pmatrix} \ell & \ell' & \nu \\ 0 & 0 & 0 \end{pmatrix} (2\nu+1) \begin{pmatrix} \nu \\ p \end{pmatrix} \begin{pmatrix} \nu+p-1 \\ \nu \end{pmatrix} x^p, \end{aligned}$$

is used to bare the common argument q_n/k . Putting now this expansion into the sum in (A3), and setting

$$\tilde{\Gamma}(\ell, \ell', \nu, p) = 2^{\nu} \begin{pmatrix} \ell & \ell' & \nu \\ 0 & 0 & 0 \end{pmatrix} (2\nu+1) \begin{pmatrix} \nu \\ p \end{pmatrix} \begin{pmatrix} \nu+p-1 \\ \nu \end{pmatrix}, \quad (\text{A4})$$

where the objects depending on ℓ, ℓ' and ν denote the Wigner $3J$ -symbols familiar from the Clebsh-Gordon coefficients, one ends up at

$$\sum_{n=n_o}^{\infty} \frac{P_{\ell}\left(\frac{q_n}{k}\right) P_{\ell'}\left(\frac{q_n}{k}\right)}{q_n} = \sum_{\nu=|\ell-\ell'|}^{\ell+\ell'} \sum_{p=0}^{\nu} \frac{\tilde{\Gamma}(\ell, \ell', \nu, p)}{k^{\nu}} \sum_{n=n_o}^{\infty} q_n^{p-1} \quad (\text{A5})$$

Using now the general formula

$$\sum_{n=n_o}^{\infty} q_n^j = \left(\frac{2i}{a_{\perp}}\right)^j \zeta\left(-\frac{j}{2}, n_o - \epsilon\right), \quad (\text{A6})$$

where the RHS of this equation is regarded as the regularized value of the diverging series on the left. Inserting now Eqs. (A6) and (A5) in Eq. (A3), while also replacing $a_{\perp} k \mapsto 2\sqrt{\epsilon+1/2}$, one ends up with

$$\begin{aligned} \mathfrak{U}_{\ell\ell'} &= \sum_{n=n_o}^{\infty} U_{\ell n} U_{\ell' n} = \\ &= (-1)^{\frac{\ell+\ell'}{2}+\sigma} \sqrt{(2\ell+1)(2\ell'+1)} \times \\ &\sum_{\nu=|\ell-\ell'|}^{\ell+\ell'} \sum_{p=0}^{\nu} \frac{\Gamma(\ell, \ell', \nu, p)}{\left(\epsilon + \frac{1}{2}\right)^{\frac{\nu+1}{2}}} \zeta\left(-\frac{p-1}{2}, n_o - \epsilon\right), \end{aligned} \quad (\text{A7})$$

where $\tilde{\Gamma}$ is redefined such that it includes the appearing powers of the imaginary unit and an additional factor of 2^{-1} from the replacement made above, thus yielding

$$\Gamma(\ell, \ell', \nu, p) = i^{p-1} 2^{-1} \tilde{\Gamma}(\ell, \ell', \nu, p) \quad (\text{A8})$$

-
- [1] T. Kinoshita, T. Wenger, and D. S. Weiss, *Science* **305**, 1125 (2004).
 [2] B. Paredes, A. Widera, V. Murg, O. Mandel, S. Fölling, I. Cirac, G. V. Shlyapnikov, T. W. Hänsch, and I. Bloch, *Nature* **429**, 277 (2004).
 [3] E. Haller, M. Gustavsson, M. J. Mark, J. G. Danzl, R. Hart, G. Pupillo, and H. C. Nägerl, *Science* **325**, 1224 (2009).
 [4] C. Chin, R. Grimm, P. S. Julienne, and E. Tiesinga, *Rev. Mod. Phys.* **82**, 1225 (2010).
 [5] S. Inouye, M. R. Andrews, J. Stenger, H. J. Miesner, D. M. Stamper-Kurn, and W. Ketterle, *Nature* **392**, 151 (1998).
 [6] T. Köhler, K. Góral, and P. S. Julienne, *Rev. Mod. Phys.* **78**, 1311 (2006).
 [7] M. Olshanii, *Phys. Rev. Lett.* **81**, 938 (1998).
 [8] T. Bergeman, M. G. Moore, and M. Olshanii, *Phys. Rev. Lett.* **91**, 163201 (2003).

- [9] V. A. Yurovsky, M. Olshanii, and D. S. Weiss, *Advances In Atomic, Molecular, and Optical Physics* **55**, 61 (2008).
- [10] V. Dunjko, M. G. Moore, T. Bergeman, and M. Olshanii, *Advances In Atomic, Molecular, and Optical Physics* **60**, 461 (2011).
- [11] E. Haller, M. J. Mark, R. Hart, J. G. Danzl, L. Reichsöllner, V. Melezhik, P. Schmelcher, and H. C. Nägerl, *Phys. Rev. Lett.* **104**, 153203 (2010).
- [12] S. Sala, G. Zürn, T. Lompe, A. N. Wenz, S. Murmann, F. Serwane, S. Jochim, and A. Saenz, *Phys. Rev. Lett.* **110**, 203202 (2013).
- [13] B. Fröhlich, M. Feld, E. Vogt, M. Koschorreck, W. Zwerger, and M. Köhl, *Phys. Rev. Lett.* **106**, 105301 (2011).
- [14] K. Günter, T. Stöferle, H. Moritz, M. Köhl, and T. Esslinger, *Phys. Rev. Lett.* **95**, 230401 (2005).
- [15] H. Moritz, T. Stöferle, K. Günter, M. Köhl, and T. Esslinger, *Phys. Rev. Lett.* **94**, 210401 (2005).
- [16] G. Lamporesi, J. Catani, G. Barontini, Y. Nishida, M. Inguscio, and F. Minardi, *Phys. Rev. Lett.* **104**, 153202 (2010).
- [17] J. I. Kim, V. S. Melezhik, and P. Schmelcher, *Phys. Rev. Lett.* **97**, 193203 (2006).
- [18] B. E. Granger and D. Blume, *Phys. Rev. Lett.* **92**, 133202 (2004).
- [19] P. Giannakeas, F. K. Diakonov, and P. Schmelcher, *Phys. Rev. A* **86**, 042703 (2012).
- [20] M. G. Moore, T. Bergeman, and M. Olshanii, in *Journal de Physique IV (Proceedings)*, Vol. 116 (EDP sciences, 2004) pp. 69–86.
- [21] S. Saeidian, V. S. Melezhik, and P. Schmelcher, *Phys. Rev. A* **77**, 042721 (2008).
- [22] S. Saeidian, V. S. Melezhik, and P. Schmelcher, *Phys. Rev. A* **86**, 062713 (2012).
- [23] V. S. Melezhik and P. Schmelcher, *Phys. Rev. A* **84**, 042712 (2011).
- [24] S. G. Peng, H. Hu, X. J. Liu, and P. D. Drummond, *Phys. Rev. A* **84**, 043619 (2011).
- [25] S. Sala, P. I. Schneider, and A. Saenz, *Phys. Rev. Lett.* **109**, 073201 (2012).
- [26] V. Peano, M. Thorwart, C. Mora, and R. Egger, *New Journal of Physics* **7**, 192 (2005).
- [27] V. S. Melezhik and P. Schmelcher, *New Journal of Physics* **11**, 073031 (2009).
- [28] P. Giannakeas, V. S. Melezhik, and P. Schmelcher, *Phys. Rev. Lett.* **111**, 183201 (2013).
- [29] S. Sinha and L. Santos, *Phys. Rev. Lett.* **99**, 140406 (2007).
- [30] T. M. Hanna, E. Tiesinga, W. F. Mitchell, and P. S. Julienne, *Phys. Rev. A* **85**, 022703 (2012).
- [31] D. S. Petrov and G. V. Shlyapnikov, *Phys. Rev. A* **64**, 012706 (2001).
- [32] Z. Idziaszek and T. Calarco, *Phys. Rev. Lett.* **96**, 013201 (2006).
- [33] C. Zhang and C. H. Greene, *Phys. Rev. A* **88**, 012715 (2013).
- [34] C. Zhang and C. H. Greene, arXiv:1312.6666, (2013).
- [35] X. Cui, Y. Wang, and F. Zhou, *Phys. Rev. Lett.* **104**, 153201 (2010).
- [36] P. O. Fedichev, M. J. Bijlsma, and P. Zoller, *Phys. Rev. Lett.* **92**, 080401 (2004).
- [37] Y. Nishida and S. Tan, *Phys. Rev. A* **82**, 062713 (2010).
- [38] J. I. Kim, J. Schmiedmayer, and P. Schmelcher, *Phys. Rev. A* **72**, 042711 (2005).
- [39] B. Gao, *Phys. Rev. A* **80**, 012702 (2009).
- [40] D. A. Harmin, *Phys. Rev. A* **26**, 2656 (1982); *Phys. Rev. Lett.* **49**, 128 (1982); *Comments At. Mol. Phys* **15**, 281 (1985).
- [41] C. H. Greene, *Phys. Rev. A* **36**, 4236 (1987).
- [42] M. Aymar, C. H. Greene, and E. Luc-Koenig, *Rev. Mod. Phys.* **68**, 1015 (1996).
- [43] A. Lupu-Sax, *Quantum scattering theory and applications*, Ph.D. thesis, Citeseer (1998).
- [44] L. D. Landau and E. M. Lifshits, *Quantum Mechanics: Non-relativistic Theory* (Butterworth-Heinemann, 1977).
- [45] B. Heß, P. Giannakeas, and P. Schmelcher, in preparation.
- [46] B. Gao, *Phys. Rev. A* **62**, 050702 (2000).
- [47] V. S. Melezhik, *Multi-Channel Computations in Low-Dimensional Few-Body Physics* (Springer-Verlag, Berlin, Heidelberg, 2012).
- [48] U. Fano, *Phys. Rev.* **124**, 1866 (1961).
- [49] B. Gao, *Phys. Rev. A* **58**, 4222 (1998).